On the growth of graphite lamellae in a high Si GG20 cast iron

André Paulo Tschiptschin [1]*
Wilson Luiz Guesser [2,3†]

Abstract

In this paper, observations are made on the faceted crystallographic lateral growth structure of graphite flakes in a high Si GG20 cast iron. A 3.82 wt.% Si, 3.25% wt.%C slightly hypereutectic cast iron with large type C graphite flakes embedded in a ferrite + spheroidized pearlite matrix failed catastrophically. Fracture is propagated by debonding the graphite flakes from the metallic matrix, exposing the graphite flakes' lateral surfaces on the fracture surface. Flake morphology and substructure were observed using scanning electron microscopy (SEM). Very thin and flexible triangular layers, nucleating on a "hexagonal rosette" center point, suggest a growth mechanism involving the incorporation of new carbon add-atoms. Epitaxial precipitation of secondary graphite during solid-state transformation shows a preferred growth habit in the a-direction, producing 2-D sheets of graphene to which carbon atoms can easily attach. Furthermore, the spiral growth of individual sheets, contributing to the thickening of the flake in the c-direction, could be inferred. The results are discussed, considering that graphite crystalline defects may play a decisive role in the spiral growth mechanism and the thickening of the graphite flake during solid-state secondary graphite precipitation.

Keywords: Graphite; Graphene; Grey cast iron, Growth of secondary graphite.

1 Introduction

During the construction of one of the subway lines in São Paulo City, the output connection of a large winch motor-reducer assembly broke down catastrophically. As a result, two pieces of the broken part were projected on a neighboring family home near the construction work. The slightly hypereutectic DIN 1596 - GG 20 cast iron contained large type C graphite flakes embedded in a ferrite + spheroidized pearlite matrix. Fracture is propagated by debonding the graphite flakes from the metallic matrix, exposing the graphite flakes' lateral surfaces on the fracture surface.

The two broken pieces were sent to our laboratories to conduct a failure analysis of the connection. When carrying out the fracture analyses of the gray cast iron in a Scanning Electron Microscope, we came across beautiful images of graphite lamellae on the fracture surface of the broken piece. Immediately, it came to mind that the observed graphite morphology could add new information on the growth mechanisms of graphite in a slightly hypereutectic gray iron.

This paper aims to describe the growth morphology of graphite lamellae in a high silicon, slightly hypereutectic GG20 gray cast iron. The observed findings on the growth morphology of the graphite flakes are discussed in light of recent advances in the literature concerning the lamellar graphite growth mechanisms in iron and nickel alloys and minerals.

Cast irons are Fe-C-Si alloys containing Mn, S, and P. The carbon above its solubility in solid iron is present as graphite in grey cast irons. It appears as interconnected flakes or platelets embedded in a metallic matrix, forming a natural composite [1].

Graphite is a $P6_3/mmc$ space group hexagonal crystal, with unit cell a = 0.2461 nm and c = 0.6708 nm. The in-plane covalent bond length is 0.142 nm. The distance between planes is 0.335 nm [2,3], characteristic of the structure of graphene, a two-dimensional honeycomb lattice made of two offset triangular lattices. The chemical bonds between the carbon atoms are sp^2 orbital hybrids, bounding three nearest neighbors 120 degrees apart. The hexagonal alpha graphite is composed of a stack of hundreds of thousands of graphene monolayers in an ABA sequence, Figure 1. How do the graphene monolayers stack one on top of another?

The growth of the graphene monolayers is much less probable in the direction normal to the monolayer (c-direction) [4]. This is because graphite grows faster along the tightly bonded a-axis directions [1010] than in the loosely bonded c-axis direction [0001], explaining the formation of graphite lamellae in grey cast iron. Thus, growth of the graphite flakes in the a-direction contributes to the lengthening of the flakes, while thickening should occur by incorporating carbon atoms in the c-direction on top of the basal planes, which is much more difficult.
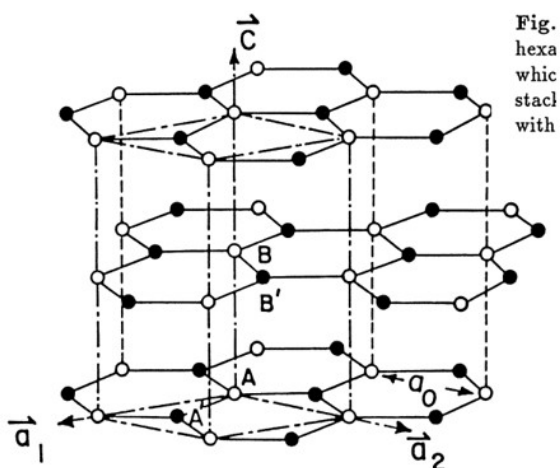
Figure 1. Crystalline structure of graphite.

Stefanescu et al. [5] discuss the growth mechanism of graphite platelets based on the incorporation of carbon atoms from graphene building blocks, resulting in hexagonal faceted graphite platelets with nanometer height and micrometer width. During solidification, thickening of the platelets occurs through the growth of additional graphene layers nucleated at the ledges of the graphite prism. As a result, graphite platelets assemble into foliated crystals and dendrites, forming graphite plates that grow along the a-axis (stage I). The growth of graphite flakes starts with the formation of 2D, one-atom-thick layers of crystalline graphite (graphene sheets) that quickly grow in the a-direction. However, to reach the multilayer structure of the graphite lamellae, the graphene sheets have to grow in the c-direction of the hexagonal cell. Amini and Abbaschian [4], studying the nucleation and growth kinetics of graphene layers from Ni-C melts, arrived at a clear relationship between the graphite interface's growth velocities and the available driving forces. Graphite's prismatic and basal interfaces are faceted low-index planes. For small driving forces, the growth of both prismatic $\{11\bar{2}0\}$ or $\{10\bar{1}0\}$ interfaces and basal interfaces $\{0001\}$ of graphene layers occur by interface-controlled faceted growth. Growth of these interfaces, in this case, takes place by lateral movement of the ledges produced by 2D-nucleation or spiral growth around a screw dislocation. For driving forces great enough to promote roughening of the lower densities prismatic interfaces $\{11\bar{2}0\}$ and $\{10\bar{1}0\}$, preferential growth of graphite in the a-directions occurs, with much higher velocities, controlled by diffusion instead of by interface.

For very high driving forces, enough to promote roughening of both prismatic and basal interfaces, the growth velocities are similar, and thickening of graphite becomes comparable to lengthening, generating spheroidal graphite.

Minkoff and Lux [6] proposed that growth of graphite occurs from steps formed on the graphite layers related to the presence of screw dislocations with Burgers vector $\vec{b} = $ c, formation of highly symmetrical twinning interfaces (20°48'), low angle tilt or twist boundaries, and wedge

disclinations. These crystalline defects have been reported as being responsible for the thickening of the flakes in the c-direction: the spiral growth around a center containing a screw dislocation may account for the thickening of the flake.

After completing the solidification process, where primary graphite crystallizes (stage I), cooling down to the eutectoid transformation temperature range induces secondary graphite precipitation (stage II). Finally, depending on the cooling rate, the eutectoid transformation leads to the further precipitation of graphite (stage III) due to the low carbon solubility in ferrite.

Profuse publication on graphite nucleation and growth directly from the melt in near eutectic or hypereutectic cast irons is available, but little is known about the precipitation of graphite during solid-state transformation. Precipitation of secondary graphite during stages II and III may occur by independent nucleation of individual particles or by epitaxial growth on the flakes' lateral surfaces with possible recrystallization [7].

The exposed lateral faces of the graphite flakes on the fracture surface of the broken part allowed glimpsing a few details of the solid-state secondary graphite growth and gave rise to reflection and discussion on the mechanisms of lateral growth of the graphite flakes in the studied high silicon gray cast iron.

2 Experimental

The chemical composition of the high silicon GG20 gray cast iron is given in Table 1.

The Si content is somehow out of the standard GG20 grey cast irons (2.0 to 2.9 wt.%). Besides being a strong graphitizer, increasing the volume fraction of lamellar graphite, high silicon contents promote longer graphite flakes and ferritization of the metallic matrix. The chemical composition allows calculating the carbon equivalent using the Carbon Equivalent Formula 1 given in [8].

$$CE = \%C + 0.33\,(\%Si) + 0.33\,(\%P) - 0.027\,(\%Mn) + 0.4\,(\%S) = 4.57\,wt.\% \tag{1}$$

Accordingly, the analyzed GG20 cast iron is slightly hypereutectic.

Thermocalc equilibrium calculations [9], using the TC 2019a version and the TCFE9 database (TC), were conducted to assess the volume fraction of graphite flakes formed in equilibrium with austenite, just after solidification and after cooling to room temperature. Figure 2 shows the isopleth of the Fe-C-Si-Mn phase diagram. Single-point equilibrium calculations indicated that the microstructure, just after solidification at 1160 °C, should be composed of 6 vol.% graphite and 94 vol.% austenite. After cooling down to room temperature, the graphite volume fraction may increase up to 10%, depending on the cooling rate.

Graphite primary crystals crystallize at the beginning of the solidification, before the coupled growth of graphite, which

Table 1. Chemical composition of the GG20 gray cast iron in wt.%

Fe	C	Mn	Si	P	S
92.90	3.25	0.39	3.82	0.08	0.12

Figure 2. Isopleth of the Fe-C-Si-Mn phase diagram.

Figure 3. Coupled zone and solidification of an hypereutectic grey iron. $\Delta T\gamma$ is the supercooling of the liquid phase concerning the γ phase. ΔTGr is the supercooling of the liquid phase concerning the γ phase. Adapted from López et al. [10].

generates the interconnected microstructure characteristics of grey cast iron. López et al. [10] discussed the solidification of hypereutectic melts and described the crystallization of primary graphite crystals from a supercooled hypereutectic liquid. After nucleation of the first graphite primary crystals directly from the melt, further cooling favors the growth of graphite lamellae in contact with the melt, which progressively loses carbon. Then, the liquid reaches a temperature undercooled regarding both the eutectic temperature and the austenite-graphite metastable equilibrium temperature, allowing the nucleation and growth of austenite. As austenite grows, rejecting carbon and promoting recalescence, the C concentration in the melt increases, reaching the asymmetrical coupled zone, where coupled growth occurs until all liquid is consumed, as shown in Figure 3.

The fractographic analysis of the sample was carried out in a Philips XL-30 Scanning Electron Microscope with a tungsten filament electron gun, a dedicated solid-state annular back-scattered electron detector (BSE), and an Everhart-Thornley Secondary Electron Detector (SE), operating at 20 kV and 10 mm working distance (WD). A back-scattered electron image (Figure 4) from the fracture surface showed approximately a 67% area fraction of graphite (gray constituent) and 33% of metallic matrix (white areas). Considering that the amount of graphite in equilibrium after cooling down to room temperature after solidification is not more than 10 vol.%,
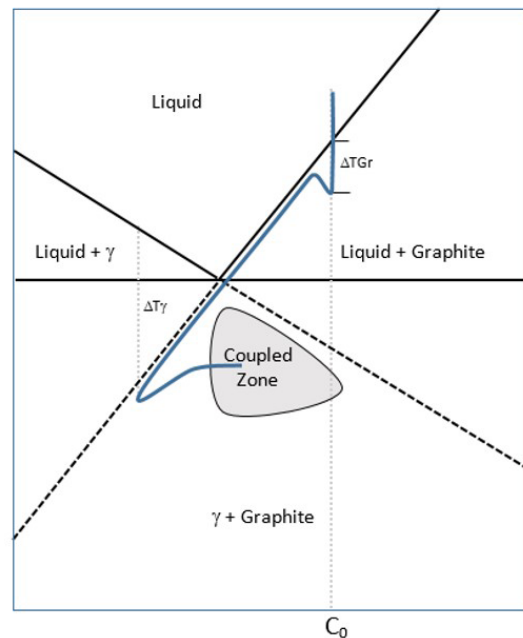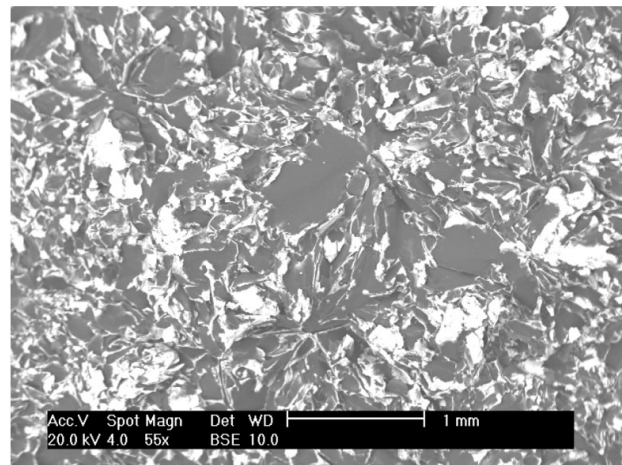

Figure 4. Back Scattered Electron Image of the fracture surface showing graphite flakes (grey area) covering 67% of the fractured area. The metal matrix appears as white areas. SEM.

the extensive coverage of the fracture surface with graphite flakes indicates that debonding of the graphite flakes from the metallic matrix occurred during fracture. In addition, the large gray areas, about 1 mm in dimension, indicate exposed individual graphite flakes on the fracture surface.

Metallographic preparation was carried out by wet grinding the specimen in successively finer SiC abrasive paper and final mechanical polishing in 6 μm, 3 μm, and 1 μm diamond paste. Nital 2% was used for etching the microstructure. Optical Microscopy (OM) Images were

taken in an Olympus BX-60 microscope with a coupled Altra 20 3 MPixel camera.

Figure 5 shows the microstructure of the analyzed specimen. A few primary graphite crystals may be seen, aside from graphite lamellae. Based on ASTM A247 standard [11], the graphite classification is type C and Class 1 size. The metallic matrix is composed of spheroidized pearlite and ferrite, indicating the precipitation of secondary graphite during cooling.

3 Results and discussion

3.1 Fractographic analysis

Figure 6 shows the fractured surface. Most of the fractured area is covered with graphite flakes indicating the fracture propagated along graphite-matrix boundaries. A dimpled ductile fracture of the metallic matrix can also be seen between the exposed graphite flakes. The light gray areas in Figure 6 correspond to the torn metallic matrix in the microstructure.

Brittle fracture propagated along the graphite-metallic matrix interfaces, exposing most graphite on the fracture surface. It could be argued that graphite could fracture by cleavage along the flat planar (0001) cleavage surfaces due to the alignment of weaker bonds between atoms in the crystal lattice. However, Bradley and Srinivasan [12] discuss graphite's dominant influence on crack propagation in grey and ductile cast irons. Damage initiates at the graphite flakes, all microcracking occurring along the graphite-ferrite interface. The graphite flake shape in gray iron causes debonding to occur at very low strain levels, giving a very low fracture toughness. Once graphite debonds from the metallic matrix, plastic deformation concentrates at the matrix bridges between graphite.

The debonding that occurred at the graphite matrix interface allowed the observation of the growth structure of graphite in greater detail.

In Figure 6, one can see a relatively smooth and undulated surface and some hairlines crossing the surface, as well.

Figures 7 and 8 allow the observation of the crystallographic character of the growth of the graphite flakes: very thin and flexible equilateral triangular layers laid on top of one another, nucleated on a "hexagonal rosette" center point, grew by incorporating new carbon atoms overlaid to those beneath them, maintaining a preferred growth habit in the a-axis direction, and producing 2-D sheets to which carbon atoms can easily attach. The hairlines seen in Figure 6 are ledges delineating the growing graphene foils. The exposed graphite lamellae on the surface may be described as hexagonal structures composed of overlapping triangles, approximately 30 to 35 μm side length, which cover all the surface of the graphite flake.

The growth of the graphene monolayers is much less probable in the direction normal to the monolayer (c-direction) [4]. This is because graphite grows faster along the tightly bonded a-axis directions [1010] than in the loosely bonded c-axis direction [0001]. Thus, growth of the graphite flakes in the a-direction contributes to the lengthening of the flakes, while thickening should occur by incorporating carbon atoms in the c-direction on top of the basal planes, which is much more difficult. Figure 8 brings up evidence of a spiral kind of growth of the overlaying graphene foils in the c-direction, contributing to the thickening of the graphite flake.

Once the end of solidification, the graphite flakes do not grow anymore in the A-direction. However, around 35% of the graphite remains to grow by squeezing the carbon atoms out from the austenite to the existing graphite flake surfaces when the temperature decreases from the solidus to the solid-state transformation temperature. The observed graphene monolayers were most likely formed close before the solid-state transformation and correspond well to the known literature explaining the dominant graphite growth mechanisms in the C-direction by incorporating carbon atoms on the ledges of graphene layers.
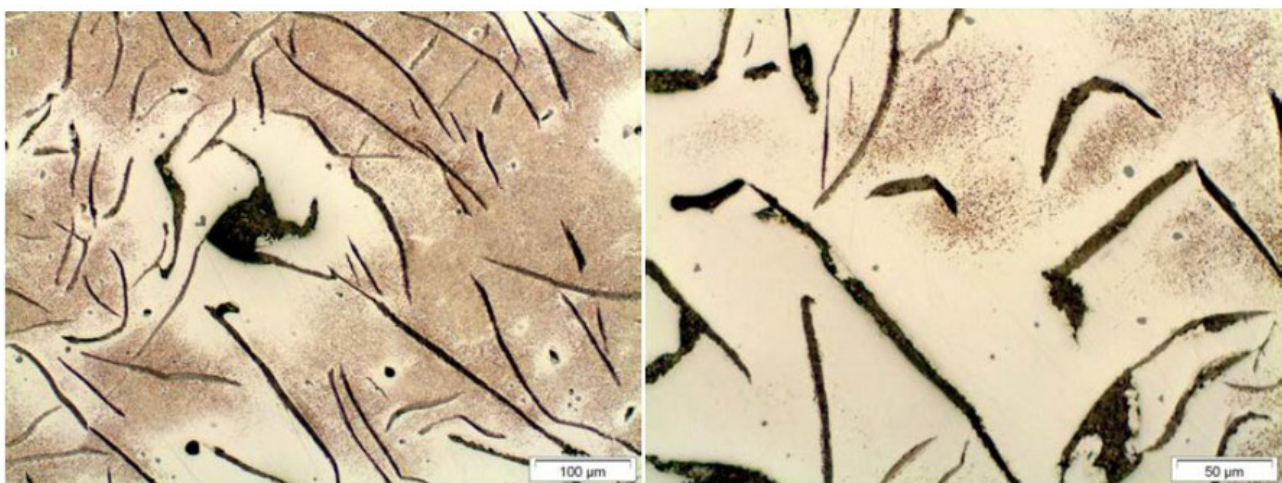

Figure 5. Microstructure of the GG20 gray cast iron. Type C graphite with large graphite primary crystals and lamellae. Ferrite plus spheroidized pearlite metallic matrix. Nital 2%.
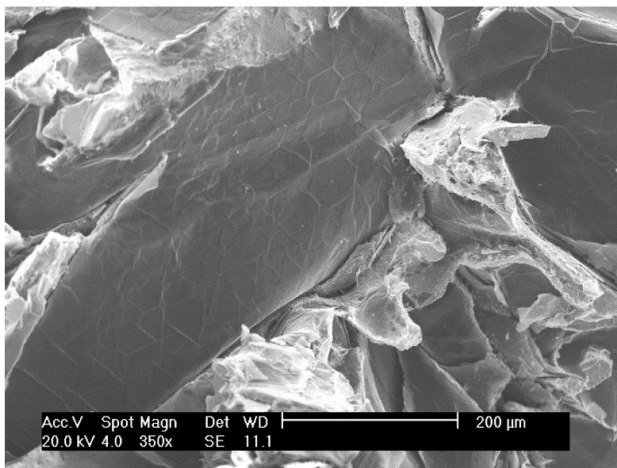
Figure 6. Secondary Electron Image shows graphite flakes' morphology exposed after the fracture. Tearing of the ferrite matrix is also seen, showing a dimpled fracture. SEM.
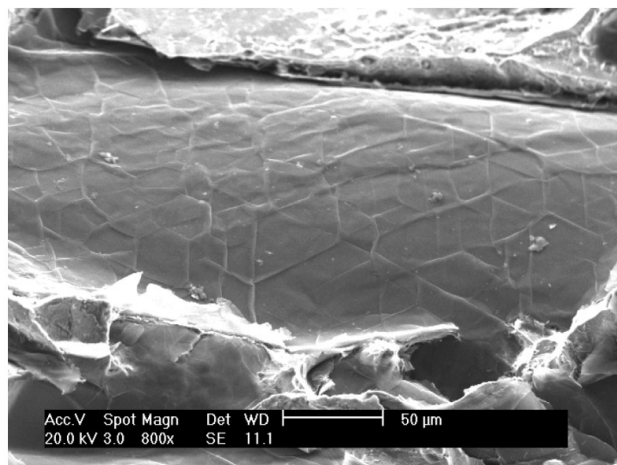

Figure 7. Secondary Electron Image of graphite flakes exposed after the fracture. SEM.
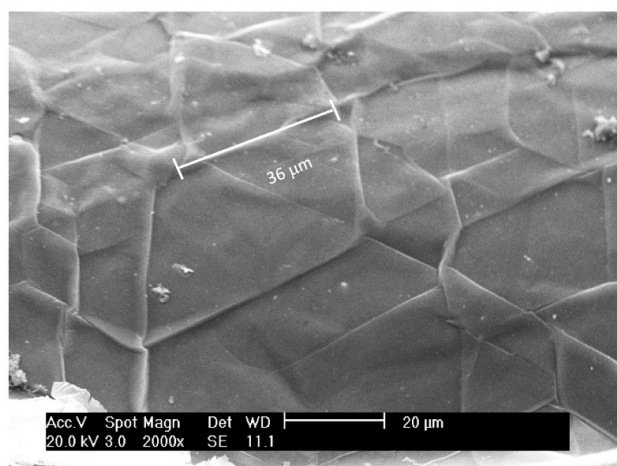

Figure 8. Secondary Electron Image of graphite flakes exposed after the fracture. SEM.

Stefanescu et al. [5] reported possible spiral growth of graphite based on micrographs taken by Guesser from a grey cast iron fractured by fatigue. The building blocks appear to be hexagonal platelets of 5 to 10 μm size stacked along the c-direction, forming the "tiled roof" structure of a foliated crystal. The orientation of the "tiled roof" structure indicates the growth direction of the lamellae, which is along the a-direction of the platelets [5].

Thermocalc calculations show that a significant volume fraction of graphite may precipitate after solidification, depending on the cooling rate. In addition, the presence of ferrite in the metallic matrix (Figure 5) indicates that precipitation of secondary graphite must have occurred. Accordingly, Figures 6 to 8 are evidence of epitaxial growth of secondary graphite wedged between the graphite flakes formed during solidification and the austenite phase [13].

Kvasnitsa et al. [14] observed very similar morphologies of flexible and thin tabular graphite crystals, grown from anorthosites gneisses, contributing to the formation of macrospirals with a negative wedge disclination, accounting for twist misorientations between graphite layers, enhancing growth in the [0001] direction. Yao and Wong [15] also reported the growth of monolayer graphene foils during atmospheric pressure Chemical Vapor Deposition and constitute clear evidence of the crystallographic character and anisotropy of surface energy of the graphite crystals. These morphologies were also shown by Double and Hellawell [16] when discussing nucleation and growth of graphite in cast irons.

4 Conclusions

Observation of the fracture surface of a high silicon, slightly hypereutectic GG20 grey cast iron allowed concluding:

1) The lateral surface of the graphite flakes exposed by debonding from the metallic matrix showed the graphite flakes' crystallographic character;

2) Hexagonal structures formed by overlapped triangular graphene layers cover the lateral surfaces of the graphite flakes;

3) Evidence of spiral growth of overlaying graphene foils in the c-direction, contributing to the thickening of the graphite flake, was shown;

4) Epitaxial precipitation of secondary graphite on the surface of graphite flakes formed during solidification is discussed based on the contribution of crystalline defects.

Acknowledgements

References

1   Cooper CA, Young RJ, Elliott R. Cast iron: a natural metal matrix composite. In: Proceedings of the ICCM Conference; Paris; 1999 July 5-9. Tours, France: ICCM; 1999.

2   Delhaes P. Graphite and precursors. Boca Raton: CRC Press; 2001.

3   Dresselhaus MS, Dresselhaus G, Surihara K, Spain IL, Goldberg IL. Graphite fibers and filaments. Berlin: Springer; 1988. (Springer Series in Materials Science; no. 5).

4   Amini S, Abbaschian R. Nucleation and growth kinetics of graphene layers from a molten phase. Carbon 2013;51:110-123.

5   Stefanescu DM, Alonso G, Larrañaga P, De la Fuente E, Suarez R. On the crystallization of graphite from liquid iron carbon silicon melts. Acta Materialia. 2016;107(1):102-126.

6   Minkoff I, Lux B. Graphite growth from metallic solution. In: Lux B, Minkoff I, Mollard F, editors. The metallurgy of cast iron. St. Saphorin, Switzerland: Georgi Publishing; 1975. p. 473-493.

7   Stefanescu DM, Alonso G. Suarez R. Recent developments in understanding nucleation and crystallization of spheroidal graphite in iron-carbon-silicon alloys. Metals. 2020;10(4):471.

8   Stefanescu DM, Lacaze J. Thermodynamics principles as applied to cast iron. In: ASM International. ASM Handbook. 1A Cast Iron Science and Technology. West Conshohocken: ASM International; 2017.

9   Andersson JO, Helander T, Höglund L, Shi PF, Sundman B. Thermo-calc and DICTRA version 2019a. Computational tools for materials science. Calphad. 2002;26(2):273-312.

10 López M, Massone JM. Boeri RE. Evolution of the macrostructure of gray cast iron from eutectic to hypereutectic composition. Materials Science Forum. 2018;925:110-117. https://doi.org/10.4028/www.scientific.net/MSF.925.110.

11 ASTM International. ASTM A247-19 - Standard Test Method for Evaluating the Microstructure of Graphite in Iron Castings. West Conshohocken: ASTM International; 2019.

12 Bradley WL, Srinivasan MN. Fracture and fracture toughness of cast irons. International Materials Reviews. 1990;35:139.

13 Diószegi A. Jönköping, SE: Jönköping University; 2022. Personal communication.

14 Kvasnistsa VN, Yatsenko VG, Jaszczak JA. Disclinations in unusual graphite crystals from anorthosites of Ukraine. The Canadian Mineralogist. 1999;37(4):951-960.

15 Yao Y, Wong CP. Monolayer graphene growth using additional etching process in atmospheric pressure chemical vapor deposition. Carbon. 2012;50(14):5203-5209.

16 Double DD, Hellawell A. The nucleation and growth of graphite—the modification of cast iron. Acta Metallurgica et Materialia. 1995;46(6):2435-2442.